

Impact Response of the Tail Beam Jack Based on Bidirectional Fluid-Structure Coupling Simulation

Yanpeng Zhu, Qingliang Zeng,* Lirong Wan, Zhe Li, and Dejian Ma



Cite This: *ACS Omega* 2023, 8, 15684–15697



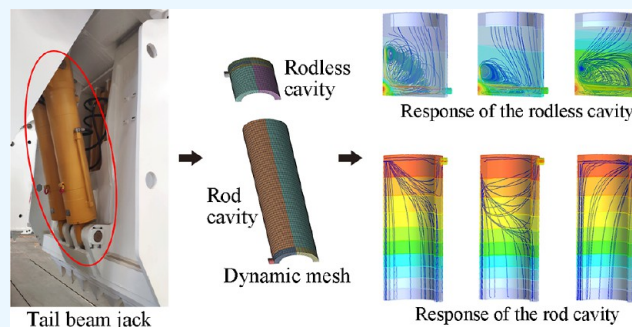
Read Online

ACCESS |

Metrics & More

Article Recommendations

ABSTRACT: In top coal caving mining, the coal rock collapse will cause an irregular impact on the tail beam jack of the caving control mechanism. The severe impact will lead to jack failure. The bidirectional fluid-structure coupling model is built on Fluent and Mechanical software to study the impact response of the tail beam jack. The dynamic flow velocity streamlines, hydraulic pressure distribution, stress field, and strain field of the jack under impact load are extracted. The response characteristics of the jack in the stationary state and motion state are analyzed. The conclusions are as follows: the stress and strain of the rodless cavity are much larger than those of the rod cavity, which is more likely to be damaged. The hydraulic pressure in the jack cavity is in vertical layered distribution. The flow velocity streamlines present spiral shapes. The response degree of the hydraulic pressure signal in the rodless cavity is stronger than that in the rod cavity, and the response degree of the flow velocity signal in the rod cavity is stronger than that in the rodless cavity. The impact response of the jack in the motion state is more sensitive and stronger than that in the stationary state. The coal rock collapse situation can be most effectively identified only by comprehensively analyzing the rodless cavity's pressure signal and the rod cavity's velocity signal. This paper innovatively visualizes the flow velocity streamlines and pressure distribution together. The bidirectional fluid-structure coupling method is innovatively applied to the tail beam jack. The findings of this study can help for better understanding of the tail beam jack's structural design and failure prevention. This study provides a certain research basis for the intelligent coal rock identification technology in mining coal based on jack vibration signals.



1. INTRODUCTION

In top coal caving mining, the working environment of the hydraulic support is harsh. The top coal rock collapse will cause complex and irregular impacts on the caving control mechanism of the hydraulic support. The severe impact seriously affects the performance and reliability of the tail beam jack.¹ The tail beam jack is the primary bearing and posture control component of the caving control mechanism. It affects the bearing reliability of the mechanism and controls the opening and closing of the caving window.² The tail beam jack is a single-rod double-acting hydraulic cylinder. It converts hydraulic pressure into mechanical movement.³ At the beginning of the coal caving, the liquid is fed into the rod cavity. The piston rod retracts to control the opening of the caving window. In the caving process, the jack is closed, so the caving window is fixed. At the end of the caving, the liquid is fed into the rodless cavity. The piston rod extends to control the closure of the caving window. This process completes the coal caving round. Thus, the tail beam jack is closely related to the caving control mechanism's performance, life, and reliability. The main failure types of the tail beam jack are shown in Figure 1. It is critical to study its response

characteristic under coal rock impact load to prevent jack failure.⁴

Many scholars have studied the single-rod double-acting hydraulic cylinder. Sakai and Stramigioli⁵ simplified the numerical model of the hydraulic cylinder. They reduced the original eight-dimensional parameter space to dimensionless three-dimensional parameter space, avoiding the influence of redundant parameters. Feng et al.⁶ studied the cylinder's volume expansion failure states and the O-ring's deformation. They quantified the level of each fault factor and established a dynamic parameter response characteristic model. Deaconescu et al.⁷ proposed a method to determine the thickness of the lubrication film between seals. The problems of liquid leakage and serious friction are improved. Solazzi and Buffoli⁸ designed three new materials for cylinder blocks. The weight is reduced

Received: February 26, 2023

Accepted: April 11, 2023

Published: April 19, 2023





Figure 1. Different failure types of the tail beam jack: (a) surface wear, (b) weld crack, (c) seal breakage, (d) hydraulic oil leak, (e) piston rod bend, and (f) deformation of hinge hole.

while ensuring the performance of the hydraulic cylinder. Based on the classical Euler–Bernoulli beam theory, GómezRodríguez et al.⁹ developed a comprehensive parameter calculation model of the hydraulic cylinder. The model considers all possible influencing factors and can get more accurate analysis results. Sherje et al. analyzed the cushioning effect of different shape cushions and optimized the shape contour of the cushion of the hydraulic cylinder. Lyu et al.¹⁰ designed a hydraulic cylinder control valve with an energy recovery function to solve the energy loss problem. Qiu et al.¹¹ detected the internal leakage of the hydraulic cylinder and established an intelligent method for cylinder wear identification. In addition, many scholars have conducted mathematical analysis research on hydraulic cylinders. For example, Zhao and Wang¹² designed a multisensor monitoring scheme based on grating, pressure, and displacement and established an analysis model of the hydraulic cylinder wear characteristics. Li et al.¹³ realized the automatic detection of hydraulic cylinder leakage faults by the AdaBoost-BP method.

It can be seen that there are many single-sided studies on hydraulic cylinders, such as the strength of structure or the leakage of fluid. However, few studies comprehensively consider the bidirectional coupling between fluid and structure. When the jack works, the hydraulic oil will interact with the solid cylinder wall and piston rod.¹⁴ Especially, under the impact load of coal rock collapse, the interaction between hydraulic oil and jack structure is more complex and cannot be ignored. Therefore, it is necessary to study the impact response

of the tail beam jack based on bidirectional fluid-structure coupling. In recent years, fluid-structure coupling simulation has been applied more deeply in engineering. It includes the interactive mapping of fluid and solid solutions, which can consider the characteristics of both fluid and solid simultaneously so that the results are closer to the actual phenomenon.¹⁵ In order to explore the response characteristics of the tail beam jack under impact load, this paper establishes a bidirectional fluid-structure coupling model based on Fluent and Mechanical software. The fluid velocity streamlines, the pressure distribution, and the solid stress–strain field of the jack are studied, respectively, in the stationary closed state and the liquid supply motion state.

Based on the above discussion, this paper is the first to apply the bidirectional fluid-structure coupling method to a tail-beam jack. Both the effect of the flow field on the solid deformation and the effect of the solid deformation on the flow field are considered to make the results more accurate. In addition, this paper innovatively visualizes the flow velocity streamlines and pressure distribution together. The two are analyzed simultaneously and validated against each other to make the results reliable. It also facilitates studying the intrinsic connection between the movement pattern and pressure distribution of the hydraulic fluid in the jack. This paper comprehensively analyses the response of the tail beam jack under both the stationary state and motion state, making the applicability of the results more comprehensive. The findings of this study can help for better understanding of the tail beam jack's structural design and failure prevention. This study provides a certain research basis for the intelligent coal rock identification technology in mining coal based on jack vibration signals.

2. METHODS

2.1. Theoretical Model. Fluid-structure coupling theory calculates the interaction between moving or deformed solid and variable fluid fields. It combines the fluid domain with the solid domain for a collaborative solution. According to data transmission forms, the fluid-structure coupling is divided into unidirectional and bidirectional coupling. The data of unidirectional coupling can only be transmitted from solver A to solver B. The data of bidirectional coupling is transmitted bidirectionally. The fluid solver transmits data to the solid solver, while the solid solver transmits data to the fluid solver.¹⁶ In order to analyze the interaction mechanism between fluid and solid in the tail beam jack, the bidirectional fluid-structure coupling model is selected to solve the problem. The model is solved by the partitioned iterative coupling method,¹⁷ and its iteration sequence is shown in Figure 2. In

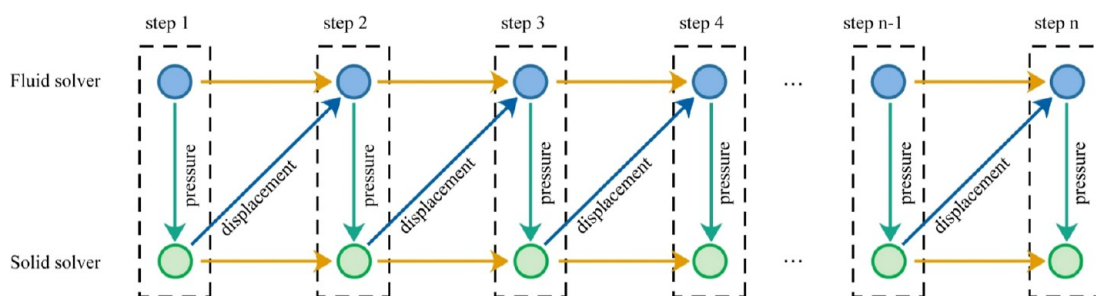


Figure 2. Iteration sequence of the bidirectional fluid-structure coupling method.

this method, the fluid and solid domains are solved once at each time step. The hydrodynamic pressure of the fluid is transmitted to the solid domain, and the motion of the structure is transmitted to the fluid domain. With this iteration, the solution of the fluid-structure coupling method is realized.

The fluid-structure coupling method should follow the three basic conservation laws of mass, energy, and momentum,¹⁸ as follows

$$\frac{\partial(\rho\varphi)}{\partial t} + \text{div}(\rho u\varphi) = \text{div}(\Gamma \text{grad } \varphi) + s \quad (1)$$

where ρ is the mass density; φ is a universal variable, which represents variables such as temperature and components of the velocity vector in different directions; Γ is the generalized diffusion coefficient; S is the generalized source term; grad represents the gradient; and div represents divergence and is defined as

$$\text{div}(a) = \frac{\partial a_x}{\partial x} + \frac{\partial a_y}{\partial y} + \frac{\partial a_z}{\partial z} \quad (2)$$

At the fluid-structure coupling interface, such as the contact surface between hydraulic oil and cylinder wall, it should also follow the conservation laws¹⁹

$$\begin{cases} \tau_f n_f = \tau_s n_s \\ x_f = x_s \\ q_f = q_s \\ T_f = T_s \end{cases} \quad (3)$$

where τ_f and τ_s are the stress of fluid and solid, x_f and x_s are the deformation of fluid and solid, q_f and q_s are the heat flow of fluid and solid, and T_f and T_s are the temperature of fluid and solid, respectively.

The following physical conservation equation should also be satisfied when solving the fluid^{20,21}

$$\begin{cases} \frac{\partial \rho_f}{\partial t} + \nabla \cdot (\rho_f \nu) = 0 \\ \frac{\partial \rho_f \nu}{\partial t} + \nabla \cdot (\rho_f \nu \nu - \tau_f) = f_f \end{cases} \quad (4)$$

where t is the time, ρ_f is the fluid density, ν is the velocity vector, f_f is the volume force vector, and τ_f is the shear force tensor.

The following governing equation should be satisfied when solving the solid

$$M_s \frac{d^2 x}{dt^2} + C_s \frac{dx}{dt} + K_s x + \tau_s = 0 \quad (5)$$

where M_s is the mass matrix, C_s is the damping matrix, K_s is the stiffness matrix, and τ_s is the stress on the solid.

2.2. Simulation Model. ANSYS Fluent^{22,23} is the fluid solver, and ANSYS Mechanical²⁴ is the solid solver. The bidirectional fluid-structure coupling model of the tail beam jack is established by combining them. The flow chart of the fluid-structure coupling simulation is shown in Figure 3.

At each time step of the simulation, Fluent transmits pressure parameters to Mechanical, and Mechanical transmits displacement parameters to Fluent, as shown in Figure 2. Bidirectional fluid-structure coupling calculation requires frequent data exchange between fluid and solid, which makes

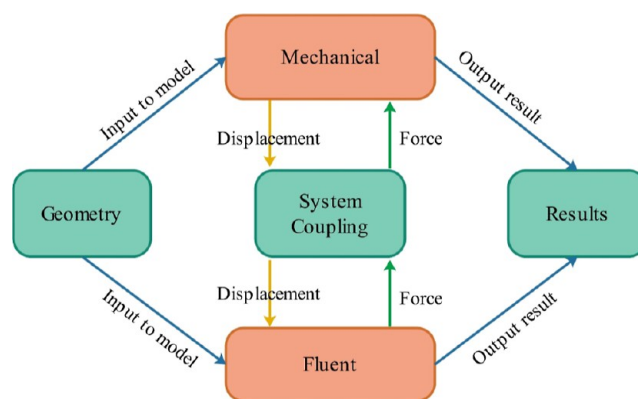


Figure 3. Flow chart of the bidirectional fluid-structure coupling simulation.

the computation costly. The jack model is simplified appropriately to reduce the amount of calculation and avoid the influence of redundant factors on the simulation results. Since the jack model is symmetric, half of the model is taken for the fluid-structure coupling model, as shown in Figure 4.

The jack model is imported into ANSYS Geometry, and the fluid and solid areas are partitioned and meshed. The structured mesh has higher computational accuracy and efficiency than the unstructured mesh. The 20-node quadratic hexahedral (20HEX) mesh has more nodes than the ordinary hexahedral mesh, which can shorten the simulation time and improve computational efficiency. This paper uses the MultiZone method to divide the 20HEX mesh of fluid and solid areas. Moreover, the quality of the mesh is checked and optimized to conform to simulation requirements.²⁵ The solid area has a grid cell count of 31,898 and a node count of 147,015, as shown in Figure 4c. The fluid area has a grid cell count of 39,570 and a node count of 177,027, as shown in Figure 4d. Under the impact load, the motion parameters of the tail beam jack are constantly changing, so the transient model is selected for the solution in both Fluent and Mechanical.^{26,27} The deformation of the solid also affects the shape of the fluid. In order to make the results more realistic and accurate, the dynamic mesh technology is used to continuously update the mesh parameters with time steps,²⁸ so that the deformation area of the mesh automatically adapts to the new shape. Remeshing layering is adopted for dynamic mesh updating. When the mesh is compressed or stretched beyond a threshold, it will be separated or combined before being computed to obtain accurate solution results.

The jack material is set to structural steel,²⁹ and its parameters are shown in Table 1. The symmetry feature is added to the jack split surface to solve it in the form of an internal structure. The impact load is added at the hinge hole of the jack piston rod. The hydraulic oil material³⁰ is set to high water-based oil according to the specific conditions of mining hydraulic supports. Its water content is 95%, so its material properties are close to water. The pressure and density changes of the fluid cannot be ignored, so to approach the actual working condition, the fluid is set as a compressible model. By precalculating the Reynolds number of the fluid, it can be known that the liquid is turbulent.^{31,32} So the solution model is set as the $k-\epsilon$ turbulence model.^{33,34}

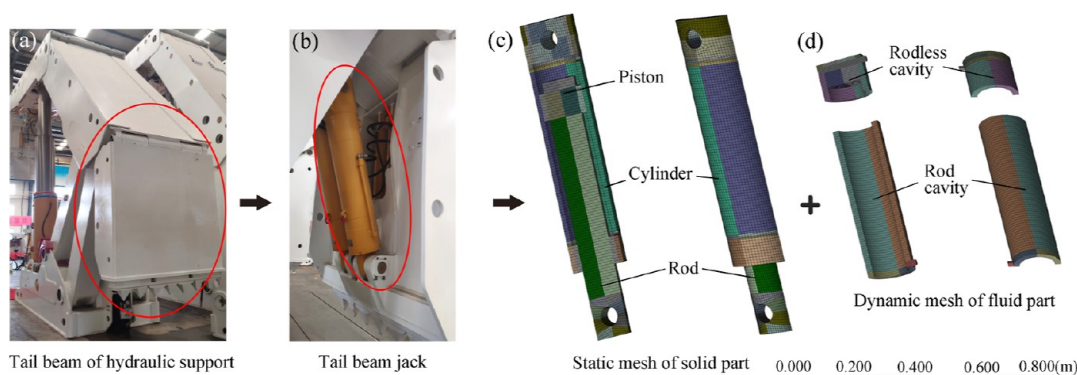


Figure 4. Structure of the tail beam jack and the mesh of solid and fluid: (a) tail beam of hydraulic support, (b) tail beam jack, (c) static mesh of the solid part, and (d) dynamic mesh of the fluid part.

Table 1. Material Parameters of Tail Beam Jack

material	tensile yield strength (MPa)	compressive yield strength (MPa)	elastic modulus (N/m ²)	density (kg/m ³)	poisson ratio
structural steel	980	835	2.06×10^{11}	7850	0.3

3. RESULTS AND DISCUSSION

3.1. Impact Response of the Tail Beam Jack in the Stationary State. In top coal caving mining, the tail beam of hydraulic support will be covered with a large number of broken top coal in the state of caving, which will produce more significant impact pressure on the jack of the tail beam. The tail beam jack in this study was taken from the ZF5600/16.5/26 hydraulic support. According to the application experience of the top coal caving hydraulic support, the load generated by the tail beam jack due to the flow impact of covering coal is set to 231.1 kN. In addition, there are small pieces of coal that randomly collapse carrying small impacts, set to 0–0.8 kN. When the tail beam jack is stationary, there is no liquid inflow or outflow in the rodless cavity and the rod cavity, so the oil port is set to the “wall” state. The force at the hinge point between the jack and the tail beam is used as input data. The force is added in the form of tabular data to the hole in the piston rod. The moment when the coal impacts the tail beam is used as the initial time. The simulation time is set to 0.05 s, and the simulation time interval to 0.0001 s. The impact load changes periodically for two cycles. The size and time of impact load are shown in Figure 5. After the simulation, the impact response characteristics are observed, such as the stress and strain of the jack and the pressure and velocity streamlines of the fluid.

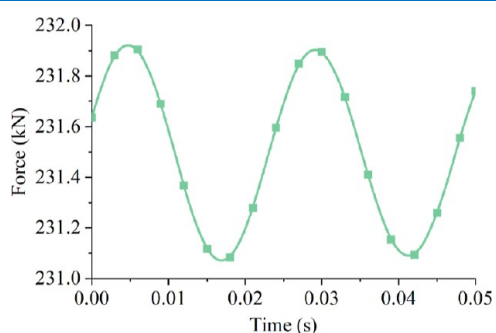


Figure 5. Impact load curve of the tail beam jack in the stationary state.

3.1.1. Stress and Strain Nephograms of the Tail Beam Jack in the Stationary State. The jack cylinder has evident stress distribution and cylinder deformation under the impact. The stress nephogram of the tail beam jack is shown in Figure 6, and the strain nephogram is shown in Figure 7.

From Figure 6, the maximum stress of the tail beam jack is 76.04 MPa, which is located on the piston and is less than the yield strength of the material. The stress concentration of the piston rod is located at the connection between the piston and the rod on the side of the rod cavity. With the stress concentration as the center, the stress gradually decreases to both sides of the piston rod. The stress concentration of the cylinder is located at the connection between the cylinder's bottom surface and the cylinder wall. There is also a certain stress concentration at the oil port. It can be observed that the stress on the side of the rodless cavity is much greater than that on the side of the rod cavity. Because the working jack is mainly thrust and support, the pressure of the rodless cavity is far greater than that of the rod cavity.

From Figure 7, the maximum deformation of the cylinder is only 5.493×10^{-6} m, which is located at the cylinder bottom and distributed on both sides above the hinge hole. The deformation of the cylinder is minimal, which meets the performance requirements and design specifications. The deformation is mainly in the rodless cavity, especially at the cylinder bottom. The strain on the rod cavity is minor, and there is no pronounced deformation. The cylinder's deformation degree is usually positively correlated with the stress, so its strain distribution is similar to the stress distribution. The deformation degree gradually decreases from inside to outside at the center of the strain concentration point on the bottom surface. As the piston rod is movable, part of its pressure is converted into displacement and compression of the liquid,³⁵ making the strain even more minor.

3.1.2. Parameter Changes of the Tail Beam Jack in the Stationary State. The working condition of the tail beam jack is mainly reflected in piston displacement, cavity pressure, and piston rod deformation. Based on the bottom surface of the piston rod as the benchmark, the piston rod deformation is calculated by the difference between the displacement of the top surface and the bottom surface, that is, the amount of compression. The piston displacement and the piston rod

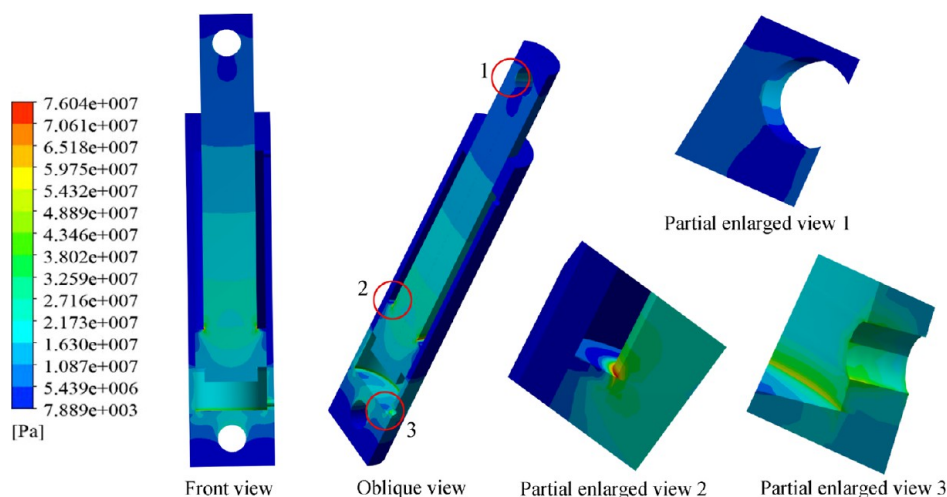


Figure 6. Stress nephogram of the tail beam jack in the stationary state.

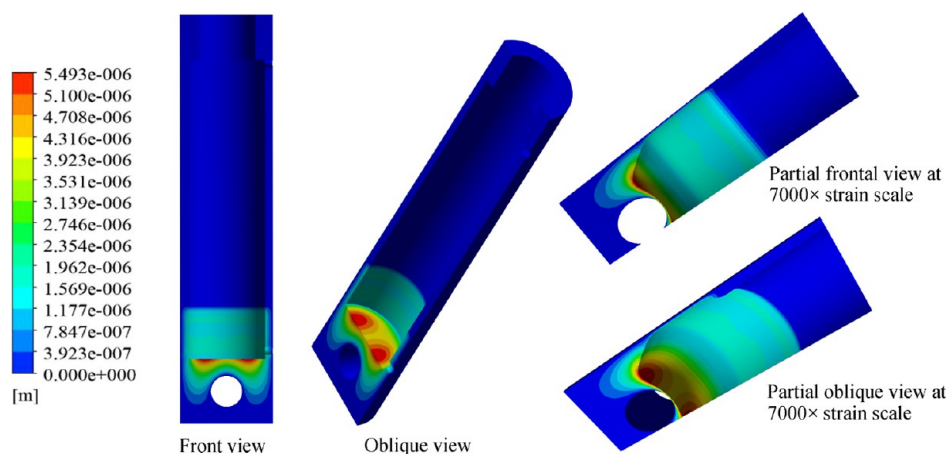


Figure 7. Strain nephogram of the tail beam jack in the stationary state.

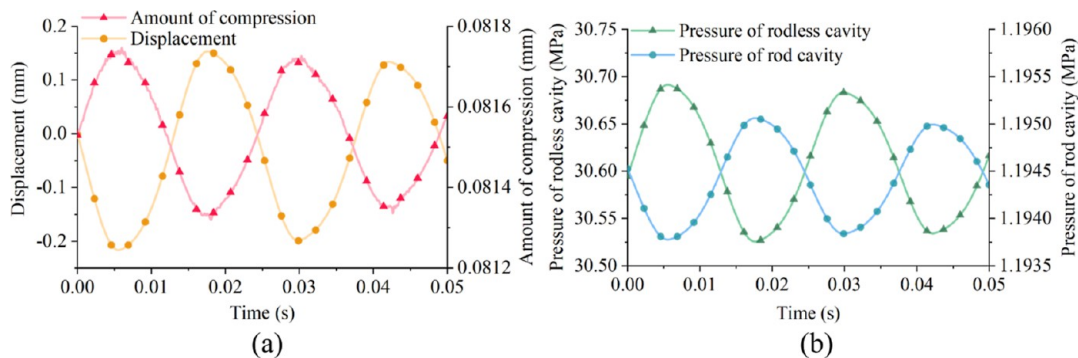


Figure 8. Parameter changes of the tail beam jack in the stationary state: (a) piston displacement and piston rod compression and (b) average pressure of the rodless cavity and the rod cavity.

compression of the jack are shown in Figure 8a. The average pressure of the rodless cavity and the rod cavity are shown in Figure 8b.

In Figure 8, the characteristic curves of the tail beam jack's displacement, compression, and pressure show similar periodic variation. From Figure 8a, during 0–0.006 s, the piston rod moves toward the rodless cavity and its axial compression degree increases. The fluid in the rodless cavity is compressed, and the fluid in the rod cavity is released. The piston rod bears considerable axial stress from the rodless cavity. In 0.006–

0.017 s, the piston rod moves toward the rod cavity and its axial compression degree decreases. The fluid in the rodless cavity is released, and the fluid in the rod cavity is compressed. The piston rod bears a more considerable axial tension from the rod cavity. Under the double action of impact load and dynamic cavity pressure, the piston rod displacement floats between -0.217 and 0.153 mm, the compression value floats between 0.08132 and 0.08174 mm, and the vibration is noticeable.

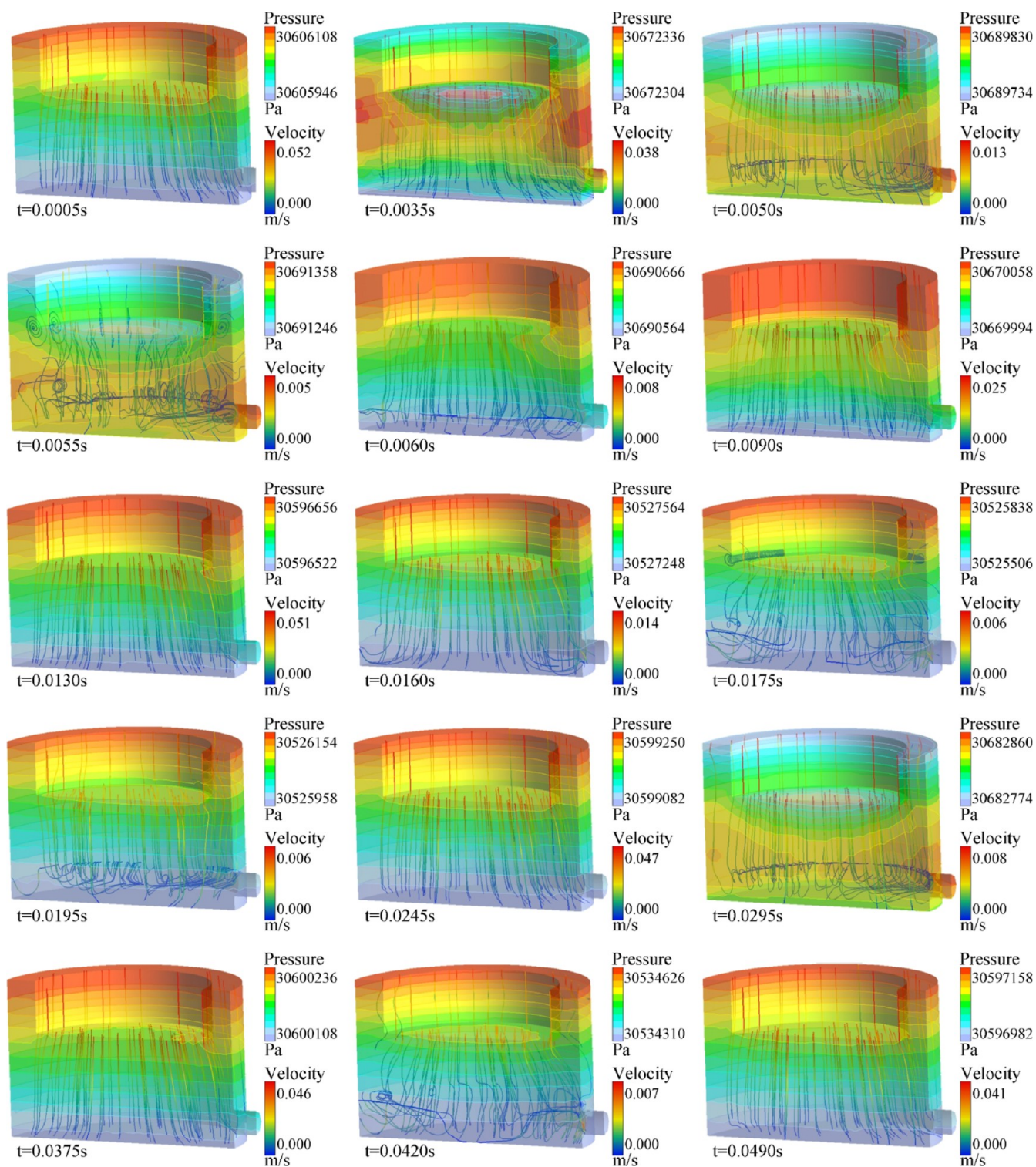


Figure 9. Pressure distribution and velocity streamline of the rodless cavity of the tail beam jack in the stationary state.

From Figure 8b, the changing trend of the average pressure in the rodless cavity and the rod cavity under the impact load is opposite. Because the total volume of the rodless cavity and the rod cavity is constant, the other will be released when one volume is compressed. The pressure in the rodless cavity vibrates up and down at 30.60 MPa. The pressure in the rod cavity vibrates up and down at 1.1947 MPa. Both have apparent pressure vibration, and the amplitude gradually decreases with the number of impacts. The pressure value in

the rodless cavity is greater than that in the rod cavity. That is because the jack is a supporting state, and the supporting force comes from the pressure difference between the rodless cavity and the rod cavity.

3.1.3. Pressure Distribution and Velocity Streamline of the Tail Beam Jack in the Stationary State. The piston rod's movement changes the jack cavity's volume, and the pressure distribution and velocity streamline change accordingly. The pressure distribution and velocity streamline in the jack cavities

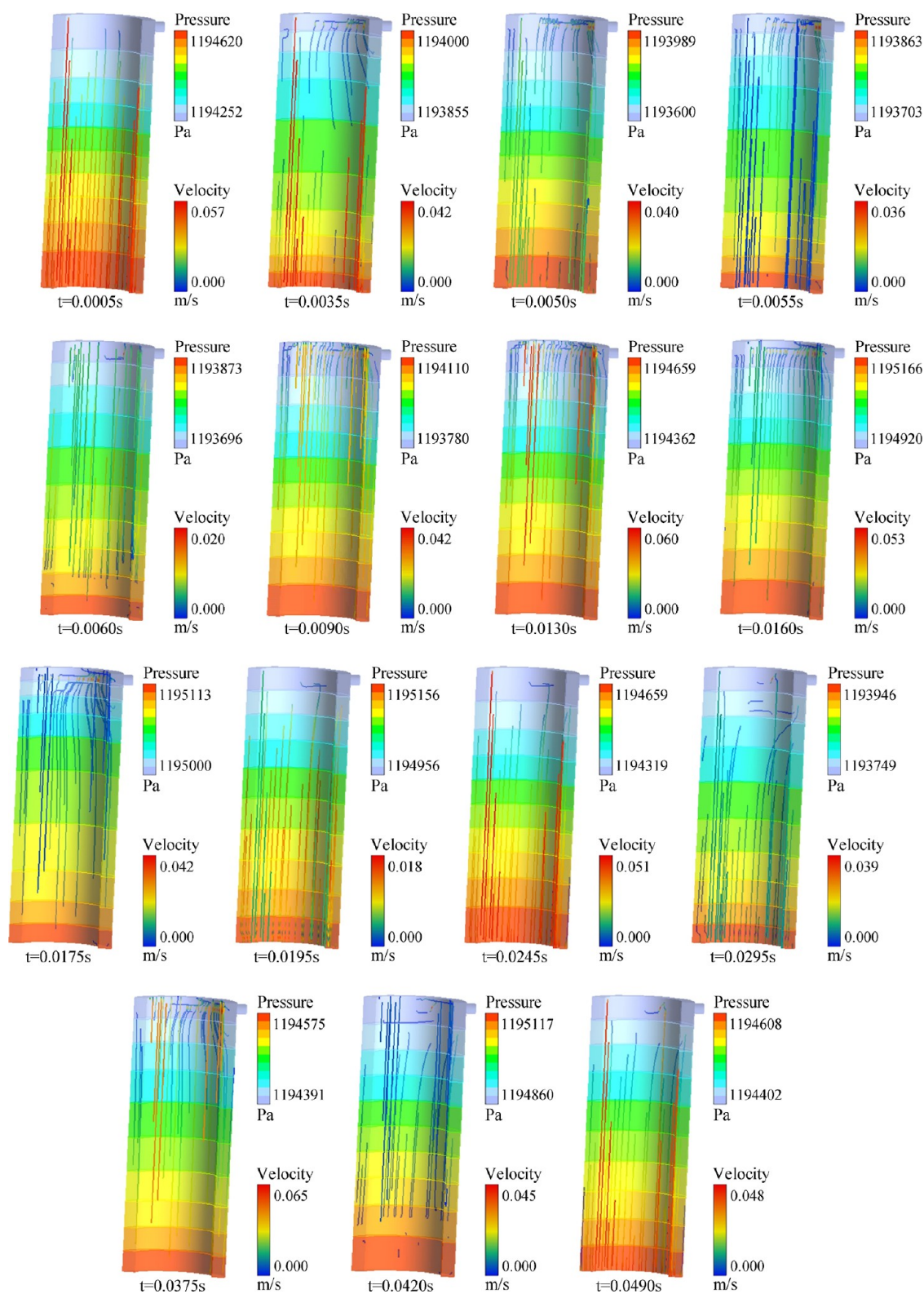


Figure 10. Pressure distribution and velocity streamline of the rod cavity of the tail beam jack in the stationary state.

at special time points are plotted, such as rise midpoint, drop midpoint, and extreme point, respectively, as shown in Figures 9 and 10.

In Figure 9, the pressure in the rodless cavity of the tail beam jack is distributed in longitudinal layers, with noticeable overall changes. At 0.0055 s, the average pressure in the rodless cavity reaches the maximum. At this time, the displacement of

the piston rod toward the rodless cavity is the largest, and the pressure difference is about 102 Pa. The pressure is maximum at the cavity bottom and decreases layer by layer along the direction of the cylinder from the bottom to the piston surface. At 0.0175 s, the average pressure in the rodless cavity reaches the minimum. At this time, the displacement of the piston rod toward the rodless cavity is the smallest, and the pressure

difference is about 320 Pa. The pressure is maximum at the piston surface and decreases layer by layer along the direction of the cavity from the piston surface to the cavity bottom. When the piston rod moves toward the rodless cavity, the average pressure in the rodless cavity rises. For example, in 0.0005–0.0055 s, the maximum pressure point gradually moves down from the piston surface to the cavity bottom. When the piston rod moves toward the rod cavity, the average pressure of the rodless cavity decreases. For example, in 0.006–0.018 s, the lower oil port releases some pressure, and the maximum pressure point returns to the piston surface and gradually decreases.

From the velocity streamline, the velocity on the piston side is always greater than that on the cavity bottom side. During 0.005–0.0055 and 0.0175–0.0180 s, the piston rod displacement approaches the maximum, and the movement direction of the piston turns. At this time, the spiral velocity streamline appears at the cavity bottom, similar to the turbulent flow state.^{36,37} At 0.0005 and 0.0130 s, the displacement of the rodless cavity is 0, and the movement direction of the piston is unchanged. At this time, the velocity streamline is gentle, similar to a laminar flow state. The second period's (0.0245–0.0490 s) pressure distribution and velocity streamline law are similar to the first period's.

From Figure 10, the pressure level in the rod cavity of the tail beam jack is distributed in longitudinal layers. The pressure change is not noticeable compared with the rodless cavity. 0.0055 and 0.0295 s are the minimal value points of pressure in the rod cavity. This is also the minimum displacement point of the piston rod toward the rod cavity. The pressure difference in the cavity is slight. The pressure is smaller in the middle of the cavity and larger in both ends. 0.0175 and 0.042 s are the maximum value points of the average pressure in the rod cavity. This is the maximum displacement point of the piston rod toward the rod cavity. The pressure difference in the cavity is significant. The pressure is larger in the cavity top and smaller in the bottom. The increase or decrease of the impact load will cause the increase or decrease of the displacement of the piston rod toward the rodless cavity. The average pressure in the rod cavity decreases gradually when the piston rod moves toward the rodless cavity, such as 0.0005–0.0055 s. When the piston rod moves toward the rod cavity, it gradually rises, such as 0.006–0.018 s. The pressure on one side of the piston surface is always larger than the pressure on the top side of the cavity. The pressure is maximum at the piston surface and decreases layer by layer along the cavity direction from the piston surface to the top of the cavity.

From the velocity streamline, the maximum velocity in the rod cavity is 0.06 m/s. The velocity streamlines at the top of the cavity are relatively disordered and those at the piston surface are relatively regular. The fluid velocity in the rod cavity is larger than that in the rodless cavity. When the piston rod displacement approaches the maximum, the movement direction of the piston turns, such as 0.0035–0.0055 s and 0.0175–0.0180 s. At this time, intensive arc-shaped velocity streamlines appear on the top of the rod cavity, and its formation time is slightly earlier than that of the rodless cavity. When the movement direction of the piston is constant, the velocity streamline is gentle, such as 0.0005 and 0.0130 s. The second period's (0.0245–0.0490 s) pressure distribution and velocity streamline law are similar to those of the first period's.

In summary, when the tail beam jack is impacted by coal rock in a closed state, the pressure distribution response is

more pronounced in the rodless cavity, and the velocity streamlines response is more pronounced in the rod cavity.

3.2. Impact Response of the Tail Beam Jack in the Motion State. This section studies the jack's vibration response of the moving mechanism under the impact of coal rock. The lifting movement of the caving control mechanism is taken as an example. The jack must overcome the covering coal pressure to move, so the liquid pressure must be greater than the covering coal pressure. In order to keep the pressure in the cylinder similar to that in the stationary state for comparative analysis, the covering coal load is reduced to 141.7 kN compared with the stationary state. The impact of the single or small amount of coal is small, set to 0–0.8 kN. When the jack gradually supports the tail beam to do support movement, the liquid enters the rodless cavity and exits the rod cavity. Therefore, the oil port of the rodless cavity is set as the quality inlet, and the oil port of the rod cavity is set as the quality outlet. The oil stream flowing into the rodless cavity is treated as negligibly small due to the short interval between the set shocks. Jack's piston rod pushes the tail beam upward through the hinge point. As the hinge point is raised, the angle between the jack and the vertical plane increases. According to force analysis,³⁸ the supporting force of the jack needs to increase gradually to maintain stability in this process. Therefore, the continuously increasing impact load is applied to the tail beam jack. Nonetheless, the increase in impact load is also small because the impact time is very short, as shown in Figure 11. After the simulation, the impact response characteristics are observed, such as the stress and strain of the jack and the pressure and velocity streamlines of the fluid.

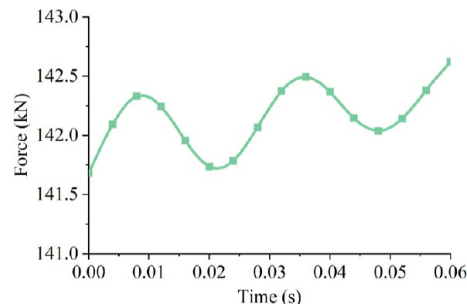


Figure 11. Impact load curve of the tail beam jack in the motion state.

3.2.1. Stress and Strain Nephograms of the Tail Beam Jack in the Motion State. Stress distribution and deformation of the jack cylinder are apparent. The stress nephogram of the tail beam jack is shown in Figure 12, and the strain nephogram is shown in Figure 13.

From Figure 12, the maximum stress of the tail beam jack is 68.58 MPa, located at the piston rod's hinge hole and is less than the yield strength of the material. The stress concentration of the piston rod is located at the interface between the piston and rod on one side of the rod cavity. The stress concentration of the cylinder is located at the interface between the cylinder wall and the cylinder bottom. The stress of the rodless cavity and piston rod is larger, while the stress of the rod cavity is relatively more minor.

From Figure 13, the maximum deformation of the jack cylinder is only 3.516×10^{-6} m, located at the cylinder bottom and distributed on both sides above the hinge hole. The overall deformation of the cylinder is minimal, which meets the performance requirements and design specifications. The

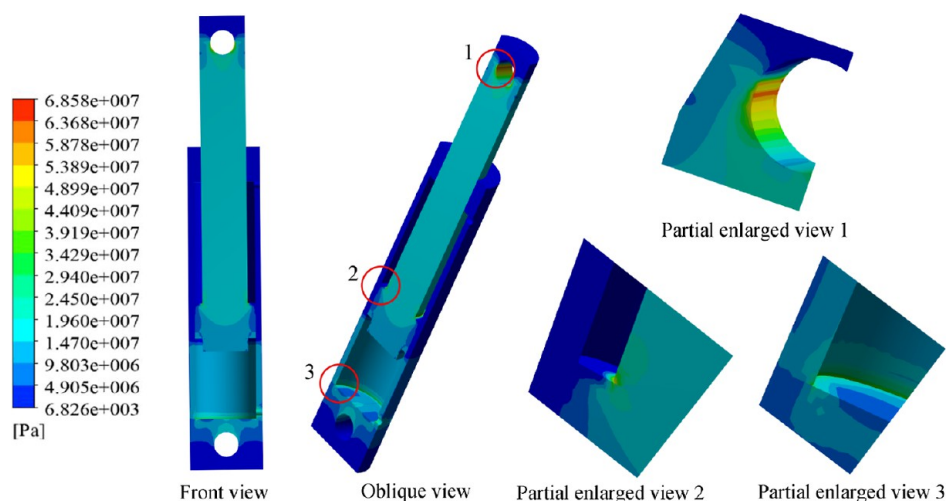


Figure 12. Stress nephogram of the tail beam jack in the motion state.

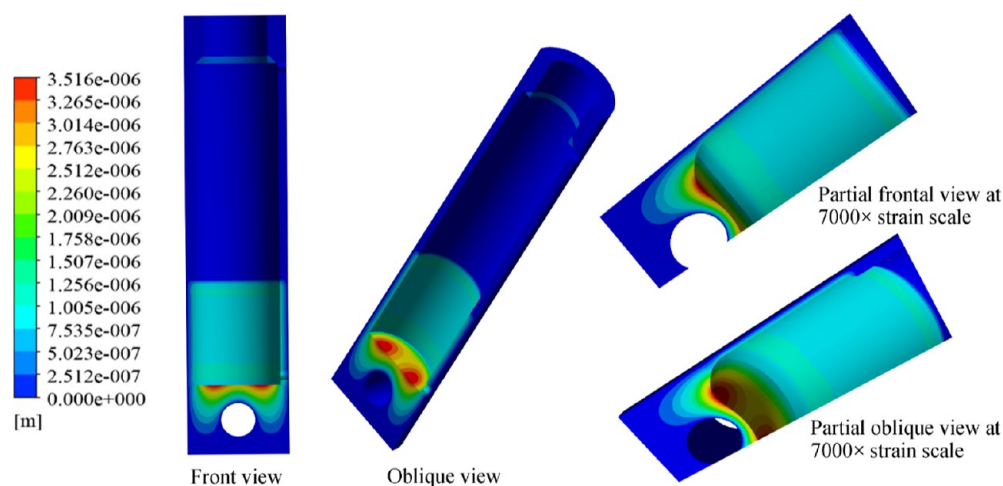


Figure 13. Strain nephogram of the tail beam jack in the motion state.

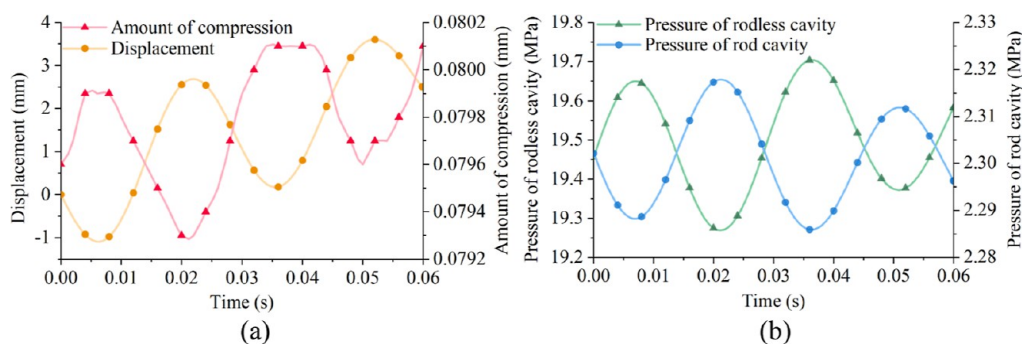


Figure 14. Parameter changes of the tail beam jack in the motion state: (a) piston displacement and piston rod compression and (b) average pressure of the rodless cavity and the rod cavity.

deformation mainly occurs on the rodless cavity and piston rod, especially on the bottom of the rodless cavity. The strain on one side of the rod cavity is minor, and there is no obvious deformation.

3.2.2. Parameter Changes of the Tail Beam Jack in the Motion State. The impact load fluctuates dynamically and increases continuously. This process covers different working conditions of the tail beam jack such as loading, bearing, and unloading. The piston displacement and piston rod compression

of the tail beam jack are shown in Figure 14a. The average pressure of the rodless cavity and rod cavity is shown in Figure 14b.

From Figure 14, the characteristic curves of the displacement, compression, and pressure show similar periodic variation. As shown in Figure 14a, the piston displacement curve is closest to the load curve, which can reflect the impact of the tail beam and the tail beam jack. The piston rod appears to have compression deformation under the double action of

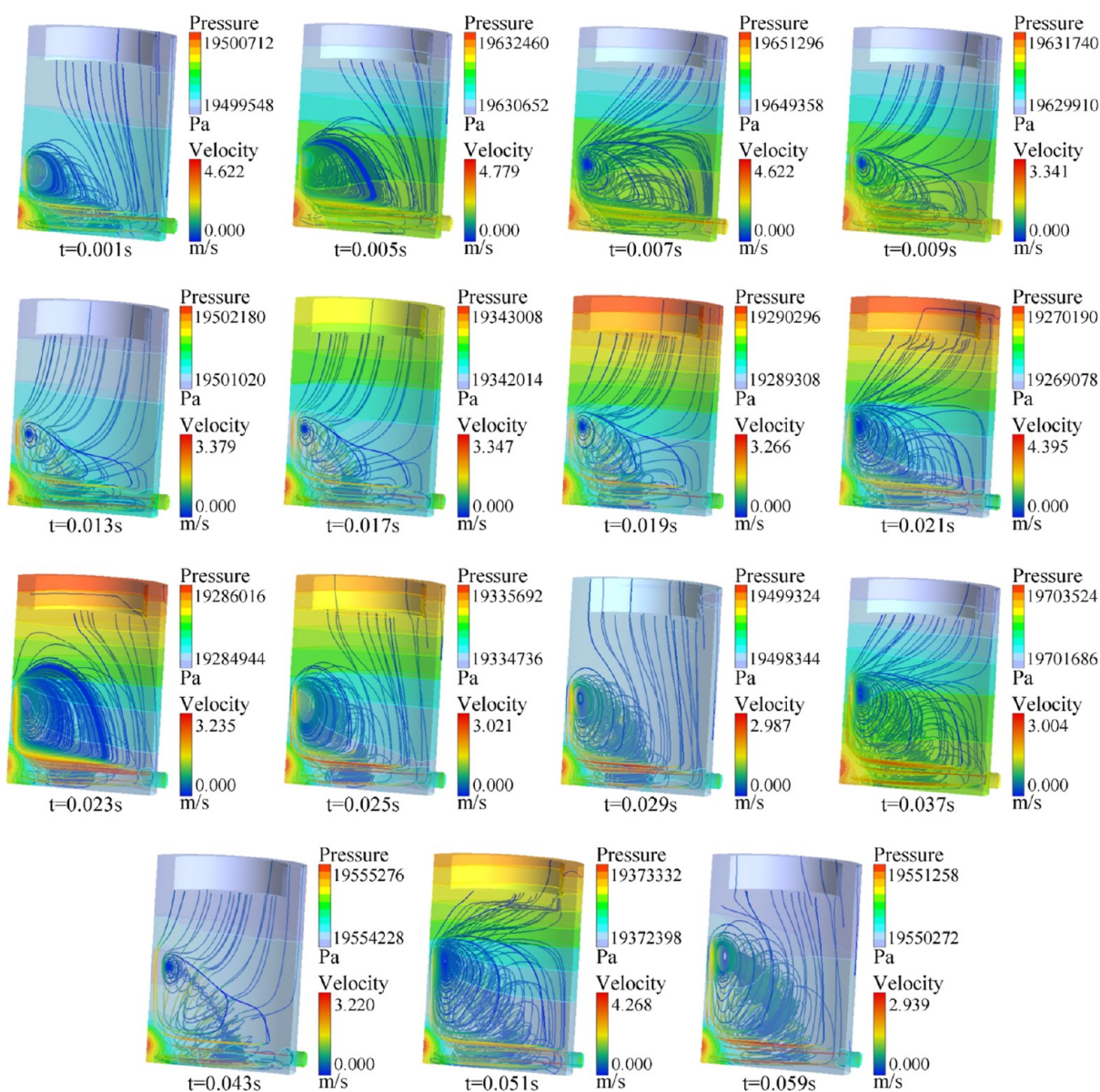


Figure 15. Pressure distribution and velocity streamline in the rodless cavity of the tail beam jack in the motion state.

external impact load and internal hydraulic pressure. With the increase of time, the median value of compression deformation fluctuation increases. As shown in Figure 14b, the pressure midline of the rodless cavity increases from 19.45 to 19.52 MPa, and the pressure midline of the rod cavity decreases from 2.302 to 2.301 MPa. The changing trend of average pressure in the rodless cavity is opposite to that in the rod cavity. The pressure in the rodless cavity tends to increase with vibration, while the pressure in the rod cavity tends to decrease with vibration. Because the jack is supported by the pressure difference between the rodless cavity and the rod cavity, such changes gradually increase the jack support force. This is consistent with the variation trend of the external load applied, which can prove that the pressure calculation is correct.

3.2.3. Pressure Distribution and Velocity Streamline of the Tail Beam Jack in the Motion State. The piston rod's movement changes the jack cavity's volume, and the pressure distribution and velocity streamline change accordingly. The pressure distribution and velocity streamline in the jack cavities at special time points are plotted, such as rise midpoint, drop

midpoint, and extreme point, respectively, as shown in Figures 15 and 16.

As shown in Figure 15, the pressure in the rodless cavity is distributed in longitudinal layers, with noticeable overall changes. Compared with the stationary state, the pressure difference in the rodless cavity is more evident in the dynamic liquid inlet and outlet state. During 0–0.007 s, the pressure in the rodless cavity increases due to the impact load. The pressure concentration in the cavity is at the cylinder wall opposite the oil port. Pressure decreases from the concentration point along the inner wall to both sides in the radial direction and from the cylinder bottom to the piston surface in the axial direction. At 0.007 s, the pressure reaches the maximum value, and the pressure difference is the maximum, 1938 Pa. During 0.007–0.021 s, the pressure in the rodless cavity decreases due to the reduction of impact load. The pressure concentration in the cavity is on the piston surface. The pressure distribution increases from the cylinder bottom to the piston surface. The second period's (0.029–0.058 s) pressure distribution and velocity streamline law are similar to

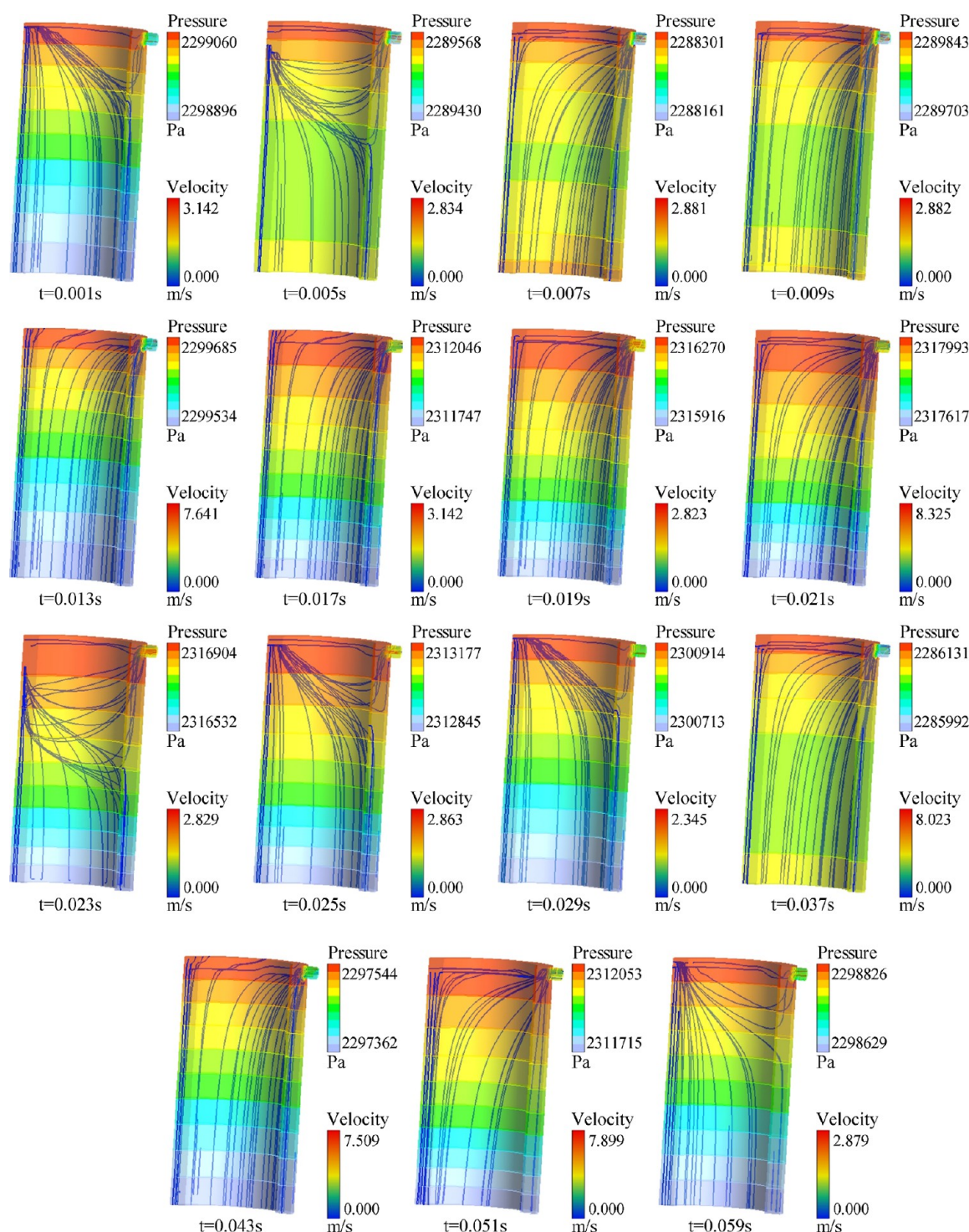


Figure 16. Pressure distribution and velocity streamline of the rod cavity of the tail beam jack in the motion state.

those of the first period's. The maximum pressure difference in the first period is 1938 Pa and that in the second period is 1838 Pa. Hence, with the increase of impact time, the pressure difference in the cavity gradually decreases, and the system gradually tends to be stable. In summary, the pressure distribution in the rodless cavity has a sensitive response to the impact load, which can reflect the magnitude and change trend of the impact load.

From the velocity streamline, the flow direction is first parallel to the oil port pipe and cylinder bottom and hits the

inner wall on the left side of the cylinder bottom. Then, it forms a complex spiral vortex^{39,40} on the left side of the cylinder bottom and turns. Finally, it flows upward along the cylinder wall to the piston and provides thrust to the piston rod through the liquid pressure. The flow velocity at the oil port and the cylinder bottom is large, while the flow velocity at the upper part and near the piston is small. It can be concluded that the spiral vortex consumes a part of the kinetic energy of the liquid, which is converted into fluid steering and cylinder deformation. During 0.007–0.021 s, the pressure in the rodless

cavity is in the decreasing stage. The piston displacement vibration is in the direction of the rod cavity. At this time, the flow velocity is high. The velocity streamlines flow out from the left side of the spiral vortex. During 0.021–0.037 s, the pressure is in the increasing stage. The piston displacement vibration is toward the rodless cavity. At this time, the flow velocity is low. The velocity streamlines enter from the right side of the spiral vortex. The liquid velocity in the rodless cavity is negatively related to the load and cavity pressure.

As shown in Figure 16, the pressure in the rod cavity of the tail beam jack is distributed in longitudinal layers. Compared with the rodless cavity, the pressure difference at each time point is smaller than 380 Pa. The minimum points of the rod cavity pressure are 0.007 and 0.037 s. This is also the minimum displacement point of the piston rod toward the rod cavity. The pressure difference in the cavity is low. The pressure is smaller in the middle of the cavity and larger in both ends. The maximum points of the rod cavity pressure are 0.021 and 0.051 s. This is also the maximum displacement point of the piston rod toward the rod cavity. The pressure difference in the cavity is large. The pressure is larger in the cavity top and smaller in the bottom. The increase and decrease of the impact load will cause the increase and decrease of the displacement of the piston rod toward the rodless cavity. The average pressure of the rod cavity decreases gradually when the piston rod moves toward the rodless cavity, such as 0.001–0.007 s. When the piston rod moves toward the rod cavity, it gradually rises, such as 0.007–0.021 s. In conclusion, the pressure distribution in the rod cavity has a sensitive response to the impact load, which can reflect the magnitude and change trend of the impact load.

Under the dynamic fluid-structure coupling, the velocity streamlines in the rod cavity are very sensitive to the increase and decrease of impact load. The velocity streamline extends smoothly from the piston to the oil port. It can be seen that during 0.007–0.021 s and 0.037–0.051 s, the impact load decreases, and the piston displacement vibration moves toward the rod cavity. The velocity streamline flows rapidly from the piston surface to the cylinder top and then flows to the oil port after colliding with the top wall. Finally, it forms an obvious semicircle arc streamline on the upper part of the cylinder. During 0–0.007, 0.021–0.037, and 0.051–0.059 s, the impact load increases, and the piston displacement vibration moves toward the rodless cavity. The velocity streamlines flow smoothly and slowly from the piston surface to the oil port, without forming a semicircle arc streamline. Compared with the rodless cavity, the response of the velocity streamlines in the rod cavity to the impact load is more evident and regular. The velocity streamline of the rod cavity can reflect the changing trend of the impact load.

In summary, when the tail beam jack is impacted by coal rock in the motion state, the response of pressure and velocity in the rodless cavity and the rod cavity are both sensitive and prominent. The response degree of the pressure in the rodless cavity is more significant than that in the rod cavity. The response degree of the velocity in the rod cavity is more significant than that in the rodless cavity. Comparative analysis shows that the response differentiation degree of the tail beam jack in the motion state is more significant than that of the tail beam jack in the stationary state.

4. CONCLUSIONS

This paper establishes a bidirectional fluid-structure coupling model of the tail beam jack under dynamic impact load. The stress and strain fields of the jack's cylinder are studied. The pressure and velocity fields of the jack's liquid are studied. The response characteristics of the jack under impact load in the stationary state and motion state are analyzed. The conclusions are as follows:

- (1) under the impact load, the stress and strain concentrations of the jack cylinder are mainly located at the oil port, the piston rod connection, and the bottom cylinder surface. The stress and strain of the rodless cavity are much larger than the rod cavity's. Damage is more likely to occur in the rodless cavity of the tail beam jack.
- (2) The liquid pressure of the tail beam jack is distributed in longitudinal layers. The layered mode shows different conditions with the varying change of impact load. The pressure gradient is more evident in the rodless cavity than that in the rod cavity.
- (3) The liquid velocity streamlines in the jack cavities show different shapes with impact load changes. Different degrees of spiral vortices are easy to form in the rodless cavity—the greater the impact, the stronger the vortex. The rod cavity does not form the vortex due to the existence of the rod. The streamlines in the rod cavity are more smooth and easy to observe.
- (4) The rodless cavity is stronger in the response degree of pressure signal, while the rod cavity is stronger in the response degree of velocity signal. To effectively identify the impact load change, it is necessary to analyze the rodless cavity's pressure signal and the rod cavity's velocity signal.
- (5) The motion state is superior to the stationary state for the response sensitivity of the jack to the impact load. The pressure and velocity signals of the jack in the motion state can identify the load variation more accurately.

The findings of this study can help for better understanding of the tail beam jack's structural design and failure prevention. Compared with the existing studies in this field, the results of this study are more authentic, comprehensive, and intuitive. An innovative bidirectional fluid-structure coupling method is used in this study. Both the stationary state and motion state are analyzed. The flow velocity streamlines and pressure distribution are visualized together. However, this study still has limitations. The influence of friction and sealing characteristics on the impact response of the tail beam jack was not considered. Friction and sealing characteristics can also influence the results to some extent. Therefore, the bidirectional fluid-structure coupling model can consider the tail beam jack's friction and sealing characteristics in further research.

■ AUTHOR INFORMATION

Corresponding Author

Qingliang Zeng – College of Mechanical and Electrical Engineering, Shandong University of Science and Technology, Qingdao 266590, China; College of Information Science and Engineering, Shandong Normal University, Jinan 250358, China; orcid.org/0000-0002-3842-9107; Email: qlzeng@sdust.edu.cn

Authors

Yanpeng Zhu – College of Mechanical and Electrical Engineering, Shandong University of Science and Technology, Qingdao 266590, China

Lirong Wan – College of Mechanical and Electrical Engineering, Shandong University of Science and Technology, Qingdao 266590, China

Zhe Li – College of Mechanical and Electrical Engineering, Shandong University of Science and Technology, Qingdao 266590, China

Dejian Ma – College of Mechanical and Electrical Engineering, Shandong University of Science and Technology, Qingdao 266590, China

Complete contact information is available at:

<https://pubs.acs.org/10.1021/acsomega.3c01303>

Notes

The authors declare no competing financial interest.

ACKNOWLEDGMENTS

This work was supported by the National Natural Science Foundation of China (grant nos. 51974170 and 51674155) and Special funds for Climbing Project of Taishan Scholars.

REFERENCES

- (1) Wang, G.; Ren, H.; Zhao, G.; Zhang, D.; Wen, Z.; Meng, L.; Gong, S. Research and Practice of Intelligent Coal Mine Technology Systems in China. *Int. J. Coal Sci. Technol.* **2022**, *9*, 24.
- (2) Yang, Y.; Zeng, Q. Impact-Slip Experiments and Systematic Study of Coal Gangue “Category” Recognition Technology Part I: Impact-Slip Experiments between Coal Gangue Mixture and Top Coal Caving Hydraulic Support and the Study of Coal Gangue “Category” Recognition Technology. *Powder Technol.* **2021**, *392*, 224–240.
- (3) Jaiswal, S.; Sopanen, J.; Mikkola, A. Efficiency Comparison of Various Friction Models of a Hydraulic Cylinder in the Framework of Multibody System Dynamics. *Nonlinear Dyn.* **2021**, *104*, 3497–3515.
- (4) Solazzi, L.; Buffoli, A. Telescopic Hydraulic Cylinder Made of Composite Material. *Appl. Compos. Mater.* **2019**, *26*, 1189–1206.
- (5) Sakai, S.; Stramigioli, S. Visualization of Hydraulic Cylinder Dynamics by a Structure Preserving Nondimensionalization. *IEEE/ASME Trans. Mechatron* **2018**, *23*, 2196–2206.
- (6) Feng, H.; Du, Q.; Huang, Y.; Chi, Y. Modeling Study on Stiffness Characteristics of Hydraulic Cylinder under Multi-Factors. *Stroj. Vestn./J. Mech. Eng.* **2017**, *63*, 447.
- (7) Deaconescu, A.; Deaconescu, T. Tribological Behavior of Hydraulic Cylinder Coaxial Sealing Systems Made from PTFE and PTFE Compounds. *Polymers* **2020**, *12*, 155.
- (8) Solazzi, L.; Buffoli, A. Fatigue Design of Hydraulic Cylinder Made of Composite Material. *Compos. Struct.* **2021**, *277*, 114647.
- (9) GómezRodríguez, V.; CabelloEras, J. J.; Hernandez Herrera, H.; GoytisoLoEspinoSa, R. Static Analysis of a Single Stage Hydraulic Cylinder. *Int. J. Eng. Technol.* **2016**, *8*, 2443–2451.
- (10) Lyu, L.; Chen, Z.; Yao, B. Energy Saving Motion Control of Independent Metering Valves and Pump Combined Hydraulic System. *IEEE/ASME Trans. Mechatron.* **2019**, *24*, 1909–1920.
- (11) Qiu, Z.; Min, R.; Wang, D.; Fan, S. Energy Features Fusion Based Hydraulic Cylinder Seal Wear and Internal Leakage Fault Diagnosis Method. *Measurement* **2022**, *195*, 111042.
- (12) Zhao, X.; Wang, J. Pump-Back Effect Analysis and Wear Feature Extraction for Hydraulic Cylinder Piston Seal Based on Multisensor Monitoring. *IEEE Trans. Ind. Electron.* **2019**, *66*, 7270–7280.
- (13) Li, L.; Huang, Y.; Tao, J.; Liu, C.; Li, K. Featured Temporal Segmentation Method and AdaBoost-BP Detector for Internal Leakage Evaluation of a Hydraulic Cylinder. *Measurement* **2018**, *130*, 279–289.
- (14) Paik, K.-J.; Carrica, P. M. Fluid–Structure Interaction for an Elastic Structure Interacting with Free Surface in a Rolling Tank. *Ocean Eng.* **2014**, *84*, 201–212.
- (15) Bonheure, D.; Gazzola, F.; Sperone, G. Eight(y) Mathematical Questions on Fluids and Structures. *Atti Accad. Naz. Lincei, Rend., Cl. Sci. Fis., Mat. Nat.* **2019**, *30*, 759–815.
- (16) Gál, P. Fluid Structure Interaction Method in Assessment of Dynamic Response of VVER 440 Reactor Internals to Pressure Shock Induced by Large LOCA Accident. *25th Conference on Structural Mechanics in Reactor Technology* 2019, 9.
- (17) Liu, W.; Li, Y.; Chen, X.; Li, C. Analysis of panel flutter characteristics on shock/boundary interaction based on fluid-structure coupling. *Acta Aeronaut. Astronaut. Sin.* **2022**, *44*, 127085.
- (18) Kim, W.; Choi, H. Immersed Boundary Methods for Fluid-Structure Interaction: A Review. *Int. J. Heat Fluid Flow* **2019**, *75*, 301–309.
- (19) Liu, M.; Zhang, Z. Smoothed Particle Hydrodynamics (SPH) for Modeling Fluid-Structure Interactions. *Sci. China: Phys., Mech. Astron.* **2019**, *62*, 984701.
- (20) Bourguet, R.; Lo Jacono, D. In-Line Flow-Induced Vibrations of a Rotating Cylinder. *J. Fluid Mech.* **2015**, *781*, 127–165.
- (21) Yu, P.; Dempsey, D.; Archer, R. Techno-Economic Feasibility of Enhanced Geothermal Systems (EGS) with Partially Bridging Multi-Stage Fractures for District Heating Applications. *Energy Convers. Manage.* **2022**, *257*, 115405.
- (22) Ansys Inc. *ANSYS Fluent User's Guide*. Ansys Fluent 2013, 15317, 2498.
- (23) Matsson, J. E. *An Introduction to ANSYS Fluent 2021*; SDC Publications: New York, 2021.
- (24) Thompson, M.; Thompson, J. *ANSYS Mechanical APDL for Finite Element Analysis*; Butterworth-Heinemann, an imprint of Elsevier: Oxford, United Kingdom, 2017.
- (25) Moatamedi, M.; Khawaja, H. *Finite Element Analysis*; CRC Press: Boca Raton, 2018. 10.1201/9780429453076.
- (26) Assi, G. R. S.; Bearman, P. W.; Kitney, N. Low Drag Solutions for Suppressing Vortex-Induced Vibration of Circular Cylinders. *J. Fluid Struct.* **2009**, *25*, 666–675.
- (27) Tabatabaei, S. S.; Kheiri, M.; Dargahi, J. Dynamics and Stability of Imperfect Flexible Cylinders in Axial Flow. *J. Fluid Struct.* **2021**, *105*, 103321.
- (28) Li, J.; Qian, X.; Liu, C. Comparative Study of Different Moving Mesh Strategies for Investigating Oil Flow inside a Gearbox. *Int. J. Numer. Methods Heat Fluid Flow* **2022**, *32*, 3504–3525.
- (29) Xin, H.; Correia, J. A. F. O.; Veljkovic, M.; Zhang, Y.; Berto, F.; de Jesus, A. M. P. Probabilistic Strain-Fatigue Life Performance Based on Stochastic Analysis of Structural and WAAM-Stainless Steels. *Eng. Failure Anal.* **2021**, *127*, 105495.
- (30) Mohammadfam, Y.; Zeinali Heris, S.; Khazini, L. Experimental Investigation of Fe₃O₄/Hydraulic Oil Magnetic Nanofluids Rheological Properties and Performance in the Presence of Magnetic Field. *Tribol. Int.* **2020**, *142*, 105995.
- (31) Chen, X.; Sreenivasan, K. R. Reynolds Number Scaling of the Peak Turbulence Intensity in Wall Flows. *J. Fluid Mech.* **2021**, *908*, R3.
- (32) Dey, K. K. Dynamic Coupling at Low Reynolds Number. *Angew. Chem., Int. Ed.* **2019**, *58*, 2208–2228.
- (33) Cho, J. R.; Chung, M. K. $AK-\epsilon-\gamma$ equation turbulence model. *J. Fluid Mech.* **1992**, *237*, 301–322.
- (34) Gallo-Méndez, I.; Moya, P. S. Langevin Based Turbulence Model and Its Relationship with Kappa Distributions. *Sci. Rep.* **2022**, *12*, 2136.
- (35) Sun, Z.; Huang, B.; Liu, Y.; Jiang, Y.; Zhang, Z.; Hou, M.; Li, Y. Gas-Phase Production Equation for CBM Reservoirs: Interaction between Hydraulic Fracturing and Coal Orthotropic Feature. *J. Pet. Sci. Eng.* **2022**, *213*, 110428.
- (36) Colagrossi, A.; Nikolov, G.; Durante, D.; Marrone, S.; Souto-Iglesias, A. Viscous Flow Past a Cylinder Close to a Free Surface:

Benchmarks with Steady, Periodic and Metastable Responses, Solved by Meshfree and Mesh-Based Schemes. *Comput. Fluids* **2019**, *181*, 345–363.

(37) Leroy, A.; Violeau, D.; Ferrand, M.; Joly, A. Buoyancy Modelling with Incompressible SPH for Laminar and Turbulent Flows. *Int. J. Numer. Methods Fluids* **2015**, *78*, 455–474.

(38) Yang, Z.; Sun, Z.; Jiang, S.; Mao, Q.; Liu, P.; Xu, C. Structural Analysis on Impact-Mechanical Properties of Ultra-High Hydraulic Support. *Int. J. Simulat. Model.* **2020**, *19*, 17–28.

(39) Liu, C.; Fu, S.; Zhang, M.; Ren, H. Time-Varying Hydrodynamics of a Flexible Riser under Multi-Frequency Vortex-Induced Vibrations. *J. Fluid Struct.* **2018**, *80*, 217–244.

(40) Williamson, C. H. K.; Roshko, A. Vortex Formation in the Wake of an Oscillating Cylinder. *J. Fluid Struct.* **1988**, *2*, 355–381.